

# Discriminating Neoplastic and Normal Brain Tissues *in Vitro* Through Raman Spectroscopy: A Principal Components Analysis Classification Model

Ricardo Pinto Aguiar, MSc,<sup>1</sup> Landulfo Silveira, Jr., PhD,<sup>1</sup> Edgar Teixeira Falcão, MD,<sup>2</sup>  
Marcos Tadeu Tavares Pacheco, PhD,<sup>1</sup> Renato Amaro Zângaro, PhD,<sup>1</sup>  
and Carlos Augusto Pasqualucci, MD, PhD<sup>3</sup>

## Abstract

**Background and objective:** Because of their aggressiveness, brain tumors can lead to death within a short time after diagnosis. Optical techniques such as Raman spectroscopy may be a technique of choice for *in situ* tumor diagnosis, with potential use in determining tumor margins during surgery because of its ability to identify biochemical changes between normal and tumor brain tissues quickly and without tissue destruction. **Methods:** In this work, fragments of brain tumor (glioblastoma, medulloblastoma, and meningioma) and normal tissues (cerebellum and meninges) were obtained from excisional intracranial surgery and from autopsies, respectively. Raman spectra (dispersive spectrometer, 830 nm 350 mW, 50 sec accumulation, total 172 spectra) were obtained *in vitro* on these fragments. It has been developed as a model to discriminate between the spectra of normal tissue and tumors based on the scores of principal component analysis (PCA) and Euclidean distance. **Results:** ANOVA indicated that the scores of PC2 and PC3 show differences between normal and tumor groups ( $p < 0.05$ ) which could be employed in a discrimination model. PC2 was able to discriminate glioblastoma from the other tumors and from normal tissues, showing featured peaks of lipids/phospholipids and cholesterol. PC3 discriminated medulloblastoma and meningioma from normal tissues, with the most intense spectral features of proteins. PC3 also discriminated normal tissues (meninges and cerebellum) by the presence of cholesterol peaks. Results indicated a sensitivity and specificity of 97.4% and 100%, respectively, for this *in vitro* diagnosis of brain tumor. **Conclusions:** The PCA/Euclidean distance model was effective in differentiating tumor from normal spectra, regardless of the type of tissue (meninges or cerebellum).

## Introduction

CENTRAL NERVOUS SYSTEM (CNS) CANCERS REPRESENT ~2% of all malignancies in the Brazilian's population.<sup>1</sup> Statistics of the Brazilian National Cancer Institute indicated an incidence of ~4820 new cases of cancer of the CNS in men and ~4450 new cases in women in 2012.<sup>1</sup> Magnetic resonance imaging (MRI), computed tomography (CT), and positron emission tomography (PET) are noninvasive detection methods for brain cancer. The gold standard for confirmation of brain neoplastic disease is biopsy followed by histopathologic evaluation of the fragment, which has a risk associated with the procedure of withdrawal depending upon location. In addition, histopathologic analysis involves time between investigation, diagnosis, and information about treatment,

producing a risk to patients from medical procedures and causing delays in confirmation, with worsened prognosis. Optical spectroscopy techniques are candidates for the expanding the ability of rapid and minimally invasive diagnostic in human tissues.

Recent studies have demonstrated the possibility of using optical techniques, particularly Raman spectroscopy, in the diagnosis of pathologic changes in human tissues.<sup>2–8</sup> Raman spectroscopy is recognized as a useful tool to analyze the chemical composition of organic and inorganic materials, because of the interaction of optical radiation incident with the vibrational, rotational, and bending modes of the molecules.<sup>9</sup>

The Raman (inelastic) scattering depends upon changes in the polarizability of the molecule caused by the incident

<sup>1</sup>Biomedical Engineering Institute, Universidade Camilo Castelo Branco - UNICASTELO, Parque Tecnológico de São José dos Campos, São José dos Campos, SP, Brazil.

<sup>2</sup>Hospital São José, Irmandade da Santa Casa de Misericórdia de Ilhéus, Ilhéus, Bahia, Brazil.

<sup>3</sup>Department of Pathology, Faculty of Medicine, University of São Paulo, São Paulo, SP, Brazil.

electric field (laser), showing energy displacement as a function of the molecular bonds. The Raman spectrum comprises energy bands that are directly related to the composition and molecular "fingerprint" of the tissue.<sup>9,10</sup> Raman spectroscopy has the potential to evaluate the pathologic state of the sample by biochemical changes resulting from the neoplastic process, and to be a valuable tool in the assessment of tumor margins during surgical resection of the tumor,<sup>9,10</sup> thus saving withdrawal of margins in extensive tissue areas that histopathologically may be considered normal, and reducing the number of samples to be effectively monitored by frozen tissue histopathology during surgery.

Several studies have presented Raman spectroscopy as a tool for diagnosis of brain tumors and metastases, and correlation of the tissue morphology with the spectroscopic differences.<sup>11–18</sup> Beljebbar et al.<sup>11</sup> evaluated the potential of Raman to classify induced intracranial C6 glioblastoma tumors in mice *ex vivo* and *in vivo*; Koljenović et al.<sup>12</sup> evaluated human glioblastoma vital tissue from necrotic ones by Raman microspectroscopic mapping, and discriminated biopsy fragments using linear discriminant analysis in a method for real-time intraoperative biopsy guidance; Krafft et al.<sup>13</sup> also evaluated the ability of Raman microspectroscopic mapping and cluster analysis to discriminate gliomas and meningiomas from typical normal tissue; Kirsch et al.<sup>14</sup> evaluated the potential of brain surface Raman mapping in detecting experimental a metastatic tumor model (murine melanoma cell), enabling the localization of cortical and subcortical tumor cell aggregates; Beleites et al.<sup>15</sup> evaluated Raman maps of borderline cases using a strategy based on partial class memberships to compare soft logistic regression and linear discriminant analysis to study the borderline of gliomas from bulk samples; Krafft et al.<sup>16</sup> applied the spectral unmixing algorithm vertex component analysis (VCA) to probe cell density and cell nuclei in Raman images of primary brain tumor tissue sections, to correlate spectral and morphologic features. Leslie et al.<sup>17</sup> evaluated pediatric brain tumors (medulloblastoma and glioma) and normal brain samples through Raman spectroscopy. Using support vector machine analysis, the authors could classify spectra of normal tissue, glioma, and medulloblastoma with 96.9%, 96.7%, and 93.9% accuracy, respectively. Zhou et al.<sup>18</sup> employed resonance Raman spectroscopy at 532 nm and statistical methods (principal component analysis [PCA] and support vector machine) to discriminate stage III meningioma and grade IV glioblastoma (malignant tissues), from benign meningioma, acoustic neuroma, and pituitary adenoma (benign tissues), and normal meningeal tissue, which yielded a diagnostic sensitivity of 90.9% and specificity of 100% for identifying cancer from benign and normal brain tissue. In summary, direct analysis of the biochemical constitution of brain tissues using Raman spectroscopy methodology allows a direct, rapid, and nondestructive detection, classification, and progression of the brain diseases.

PCA is a linear orthogonal transformation of a  $p$ -dimensional to an  $m$ -dimensional space ( $m < p$ ). The coordinates of the data in the new space are uncorrelated, and the greatest amount of variance within the original data is preserved using only a few variables.<sup>19</sup> PCA is a statistical tool used to obtain the pattern of variability of the spectral characteristic of a given material based on repeating the experiment with different samples of the material under different conditions

(for instance, pathologic changes associated with diseases). The PCA calculates the spectral features of higher variance, and ranks them according to their importance in the data set. With repetition of the experiment, it is possible to check which bands are important for identifying the material (no changes or changes within a particular group) and which ones are introduced in the spectrum as a result of random noise (shot noise and cosmic rays) or randomly occurring experimental artifacts. The PCA, associated with a discriminant analysis (such as Euclidean or Mahalanobis distance, neural network analysis, or logistic regression) applied to spectral data, has been used for the diagnosis and differentiation of various types of human diseases, such as classification of normal and diseased laryngopharyngeal tissue using PCA and Mahalanobis distance,<sup>20</sup> human thyroid cell lines using PCA and neural network analysis,<sup>21</sup> human basal cell carcinoma and skin melanoma using PCA and Mahalanobis distance,<sup>22</sup> intestinal and stomach adenocarcinoma using PCA and logistic regression,<sup>23</sup> and human carotid arteries using PCA and Mahalanobis distance.<sup>24</sup>

The objective of this work was to use Raman spectroscopy to discriminate fragments of neoplastic brain tissue (glioblastoma, medulloblastoma, and meningioma) from normal tissues (meninges and cerebellum) *in vitro*, by developing a spectral model to extract most of the spectral features of brain tissues using PCA, and to discriminate tissue (pathologic from normal) using Euclidean distance applied to the PCA scores of higher differentiation among groups verified by ANOVA.

## Materials and Methods

### Brain tissue collection

The experimental procedure was approved by the Ethics in Research Committee of the Universidade Camilo Castelo Branco (Protocol. 74032/2012). Two fragments of normal cerebellum and meninges were obtained from autopsies in the Autopsy Service of the University of São Paulo (São Paulo, SP, Brazil). Specimens of glioblastoma multiforme, medulloblastoma, and two meningiomas were obtained after a neurosurgical procedure performed at Hospital São José (Ilhéus, BA, Brazil). The tumor grades were determined by histopathologic analysis according to the classification of the World Health Organization.<sup>25</sup> After they were withdrawn, fragments were placed in cryogenic tubes, immediately frozen using liquid nitrogen, and kept refrigerated at  $-80^{\circ}\text{C}$  until spectroscopy. At the time of spectral analysis, samples were placed in an aluminum sample holder and moistened with saline solution 0.9% until reaching room temperature. A small fragment ( $2 \times 2$  mm) was randomly cut and was then submitted to Raman spectroscopy. Following this, the fragment was fixed (formalin 10%), labeled, and submitted to histologic evaluation.

### Raman spectroscopy

The acquisition of the spectra was performed using a dispersive Raman spectrometer (Dimension P-1, Lambda Solutions, Inc., MA) composed of a diode laser (wavelength of 830 nm, near infrared, output power of 350 mW), a Raman probe (Vector probe, Lambda Solutions, Inc., MA) coupled to the laser and spectrometer, and a compact  $f/1.8$  spectrometer

with a Peltier-cooled ( $-75^{\circ}\text{C}$ ), back thinned, deep depleted 1034X100 CCD, with resolution of  $\sim 2\text{ cm}^{-1}$  in the spectral range of  $400\text{--}1800\text{ cm}^{-1}$ . The acquisition and storage of the spectra were done with a notebook microcomputer using the software RamanSoft (Lambda Solutions, Inc., MA), which controls, via USB, the experiment parameters such as temperature and exposure time of the detector, camera electronic gain, number of acquisitions per sample, and, also, the storage of spectra for further processing. The exposure time for obtaining the spectra was 50 sec.

The spectrometer Raman shift calibration was checked at the time of data collection. A spectrum of naphthalene was collected and the Raman shift positions of the main bands were checked against the literature;<sup>26</sup> no corrections were necessary. Despite the lower fluorescence level of brain tissues when illuminated in the near-infrared range, the remaining background fluorescence was removed by fitting and subtracting a 7th order polynomial in raw spectrum using a routine written in Matlab 5.0 (Mathworks Inc., MA). Artifacts from cosmic rays were removed manually.

A total of 172 spectra were obtained and separated into five groups according to the histology of each sample: normal tissues from the cerebellum (45 spectra) and meninges (49 spectra), and tumor glioblastoma multiforme (20 spectra), medulloblastoma (19 spectra), and meningioma (39 spectra). The mean Raman spectrum of each group was calculated using all spectra of each tissue type and plotted using the Microsoft Excel (Office 2003, Microsoft Corp., USA).

#### Discrimination analysis based on PCA

The PCA technique decomposes the spectra data set ( $A$ ), which may be composed of correlated variables, in a set of uncorrelated variables, the principal component vectors (PCs) and scores, based on the spectral variance. The PCs represent the directions of the largest variations that occur in all spectra; and a set of scaling coefficients, called scores (SCs), that represent the intensity of each PC in the particular spectrum and can be interpreted as the cosine of the angle between the observed spectrum and the PC vectors. When PCs are multiplied by SCs and then summed, one reconstructs the original spectrum. Therefore, knowing the PCs'

vectors, one can establish the importance of each PC in the formation of the spectrum of a particular sample and then use this information (presence or absence of that particular feature in one group) to classify the spectra into pre-determined categories, as each principal component is, by definition, a spectrum.

The data set was divided into four groups: one group for normal tissues and three for neoplastic ones, and then subjected to PCA (Statistics Toolbox, Matlab 5.0). After selecting the most relevant scores that showed statistically significant differences among the four groups, a discrimination algorithm was developed based on Euclidean distance applied to these scores, to classify the Raman spectra in one of the groups.

The Euclidean distance is being used as a discriminant analysis to separate the data set into classes, by determining the linear distance from a specific point to the centroid (mean) of the class to which it belongs, compared with the distance from the centroids of the neighbor groups. The Euclidean distance  $d$  follows the expression<sup>27</sup>:

$$d(x, \mu) = [(x - \mu)^T \cdot (x - \mu)]^{1/2}$$

where  $x$  is the intensity value of a particular sample point (in this case the SC) and  $\mu$  is the centroid of the group. The choice of which SC has better capacity of discrimination was made by calculating its significance level between groups (ANOVA,  $p < 0.05$ ), whereas the SCs that had the highest differences for all groups were chosen. Then, the Euclidean distance was calculated for the SCs that exhibited higher discrimination power. The Euclidean distance discrimination line was calculated using Matlab. Sensitivity, specificity, and overall accuracy diagnostics were then calculated.

## Results

### Raman spectra of normal cerebellum (white and gray), glioblastoma, and medulloblastoma

The mean Raman spectra of brain tumors glioblastoma and medulloblastoma and normal cerebellum tissues (white and gray matters) are shown in Fig. 1, and the assignments of the highlighted peaks referenced in the recent literature

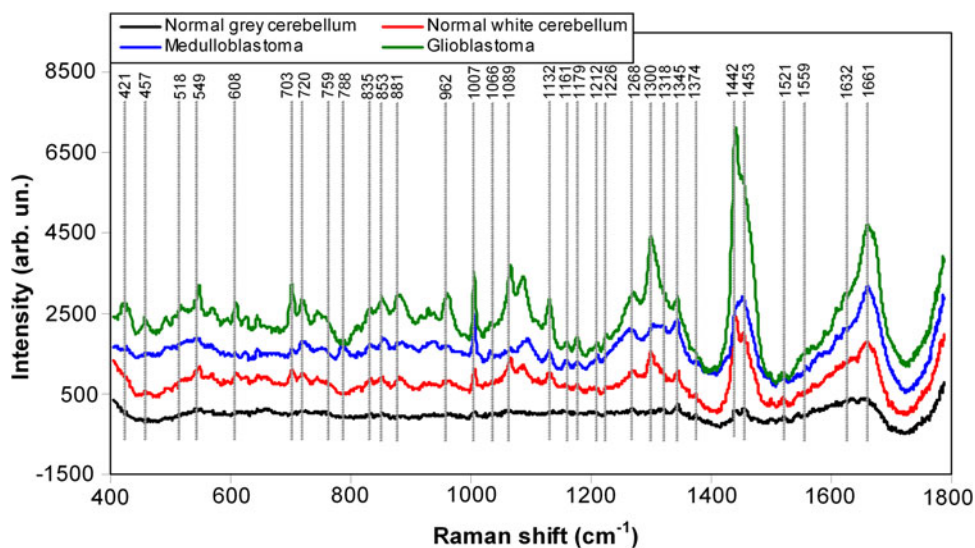


**FIG. 1.** Mean Raman spectra of normal white and gray cerebellum, glioblastoma, and medulloblastoma *in vitro*. Spectra were offset for better visualization. Wavelength, 830 nm; laser power, 350 mW; resolution,  $2\text{ cm}^{-1}$ .

are presented in Table 1.<sup>28–33</sup> The Raman peaks are correlated with the biochemical constitution of such tissues (primarily proteins, lipids/phospholipids, and cholesterol). In the spectral range of 500–1000  $\text{cm}^{-1}$ , the prominent bands correspond to vibrations of proteins, lipids, and cholesterol; the range of 1160–1600  $\text{cm}^{-1}$  are vibrations that correspond predominantly to proteins, lipids, and nucleic acid, with some contribution of hemoglobin. The contribution of water, although weak in the Raman spectra, appears as a broad band  $\sim 1632 \text{ cm}^{-1}$ .

It was observed that the Raman bands of the white cerebellum are more intense than the gray one, with featuring peaks assigned to cholesterol (549, 608, 703, 853, 881, 962, 1132, 1442, and 1453  $\text{cm}^{-1}$ ), peaks assigned to lipids/phos-

pholipids (720; 1066, 1089, 1132, 1300, 1442, and 1661  $\text{cm}^{-1}$ ), and peaks attributed to proteins (853, 881, 1007, 1268, 1345, 1453, and 1661  $\text{cm}^{-1}$ ) (Table 1). The bands at 1345 and 1521  $\text{cm}^{-1}$  (assigned to amide I from proteins and to carotenoids, respectively) have similar intensities in these two tissues. The peak at 1521  $\text{cm}^{-1}$  (assigned to carotenoids) has a similar intensity in both normal cerebellum tissues. Gray cerebellum presented higher fluorescence and, therefore, lower signal-to-noise ratio.

The Raman spectrum of glioblastoma showed bands with higher intensity than medulloblastoma and normal cerebellum across the spectral range, featuring the bands with peaks at 421, 457, 549, 608, 703, 746, 835, 853, 881, 962, 1007, 1066, 1089, 1132, 1179, 1268, 1300, 1345, 1442, and 1453  $\text{cm}^{-1}$ ,

TABLE 1. POSITIONS OF PEAKS AND ASSIGNMENT OF RAMAN BANDS OF NORMAL AND NEOPLASTIC BRAIN TISSUES, WITH REFERENCES TO RECENT LITERATURE

Raman peaks	Assignment <sup>11–16,18,28–33</sup>
421	Cholesterol
457	Proteins and cholesterol
518	Phospholipids
549	Cholesterol; (S-S) disulfide stretching (collagen)
608	Cholesterol
703	Sterol ring stretch of cholesterol
720	Asymmetric stretching of choline group $\text{N}^+(\text{CH}_3)_3$ of phospholipids (sphingomyelin/phosphatidylcholine); lipids, fatty acids - HO
746	Sterol ring stretch of cholesterol
759	Phospholipids (ethanolamine), hemoglobin, sterol ring stretch of cholesterol
788	Lipids - HO
835	Lipids - $\text{CH}_2$ , HO
853	C-C stretching of proline and CCH deformation ring breathing of tyrosine (protein); sterol ring stretch of cholesterol; glycogen
881	Hydroxyproline and tryptophan (collagen); sterol ring stretch of cholesterol; asymmetric stretching of choline group $\text{N}^+(\text{CH}_3)_3$ of phospholipids (phosphatidylcholine)
939	C-C stretching (amide III) - protein
962	Sterol ring stretch of cholesterol; $\text{CH}_2$ out-of-plane bending (proteins)
1007	C-C skeletal stretching of aromatic ring - phenylalanine/tyrosine
1037	C-H in-plane deformation - phenylalanine/proline (proteins)
1066	Lipids - HO; saturated fatty acids; phospholipids (sphingomyelin/phosphatidylcholine)
1089	Phospholipids (phosphatidylcholine); unsaturated fatty acids
1097	P-O-C and $\text{PO}_2$ groups of phospholipids (mainly phosphatidylethanolamine)
1132	C-C stretching of cholesterol; saturated fatty acids - HO; phospholipids (sphingomyelin)
1161	C-C and C-N - protein stretching
1179	C-C stretching of cholesterol, fatty acids - HO
1212	Amide III; C-C tyrosine stretching, phenylalanine, tryptophan (protein); red blood cells (hemoglobin)
1226	C-H stretching - hemoglobin
1268	$\text{CH}_2$ lipids deformation (unsaturated fatty acids and phospholipids - phosphatidylcholine/phosphatidylethanolamine); some contribution from C-N and N-H stretching (amide III); thymine and adenine (ring breathing)
1300	$\text{CH}_2$ and $=\text{CH}$ bending of cholesterol; $\text{CH}_2$ deformation of saturated/unsaturated fatty acids (sharp for saturated); phospholipids (sphingomyelin/phosphatidylcholine/phosphatidylethanolamine)
1318	Proteins
1345	C-H bending of proteins
1442	$\text{CH}_2$ and $\text{CH}_3$ bending of lipids: phospholipids (sphingomyelin) and unsaturated fatty acids; cholesterol
1453	CH functional groups ( $\text{CH}_2$ and $\text{CH}_3$ ) of amino acids side chains in proteins; phospholipids (sphingomyelin)
1521	Carotenoids ( $\text{C}_{40}\text{H}_{56}$ )
1558/1560	Hemoglobin
1632	Water - HOH bending; hemoglobin; nucleic acid (DNA)
1661	Amide I (C=O stretching of peptide backbone); C=C stretching of lipids (unsaturated fatty acids and some contribution from cholesterol [ $1674 \text{ cm}^{-1}$ ])

attributed to proteins, lipids/phospholipids, and cholesterol (Table 1). The bands at 1226 and 1560  $\text{cm}^{-1}$ , attributed to hemoglobin, present higher intensity in glioblastoma, not being found in medulloblastoma or in normal tissue in the cerebellum. Medulloblastoma, in turn, appeared with bands at 1035 and 788  $\text{cm}^{-1}$ , not seen in glioblastoma or in normal tissue, which can be attributed to phospholipids and proteins, respectively.

The majority of peaks appeared with lower intensities than glioblastoma, and several of them appeared with lower intensities than normal white tissue, such as 457, 549, 608, 703, 881, 962, 1007, 1066, 1089, 1132, 1179, 1268, 1300, and 1442  $\text{cm}^{-1}$ , with assignments primarily of lipids/phospholipids, cholesterol and proteins. The band 1521  $\text{cm}^{-1}$  (assigned to carotenoids) also has similar intensities in these two neoplasias.

#### Raman spectra of normal meninges and meningioma

Figure 2 shows the mean Raman spectra of normal meninges and meningioma. The peaks in the meninges spectra correspond to the vibrational bands attributed mainly to proteins, lipids/phospholipids, and cholesterol, as shown in Table 1. The spectrum of meningioma has higher intensity than the normal one; however, several characteristic peaks appear with higher intensity in meninges than in meningioma, such as 549, 608, 703, 759, 1066, 1300, and 1442  $\text{cm}^{-1}$ , which can be attributed to cholesterol and lipids/phospholipids. Meningioma have several peaks of higher intensity compared with the normal meninges, such as the peaks at 759, 853, 939, 1007, 1037, 1161, 1268, 1318, 1453, 1632, and 1661  $\text{cm}^{-1}$ , which can be attributed to protein, lipids/phospholipids (ethalonamine), and hemoglobin (Table 1). The bands at 788, 1212, and 1560  $\text{cm}^{-1}$  (lipids and hemoglobin) appeared only in the meningioma, compared with normal meninges.

#### Discrimination based on PCA

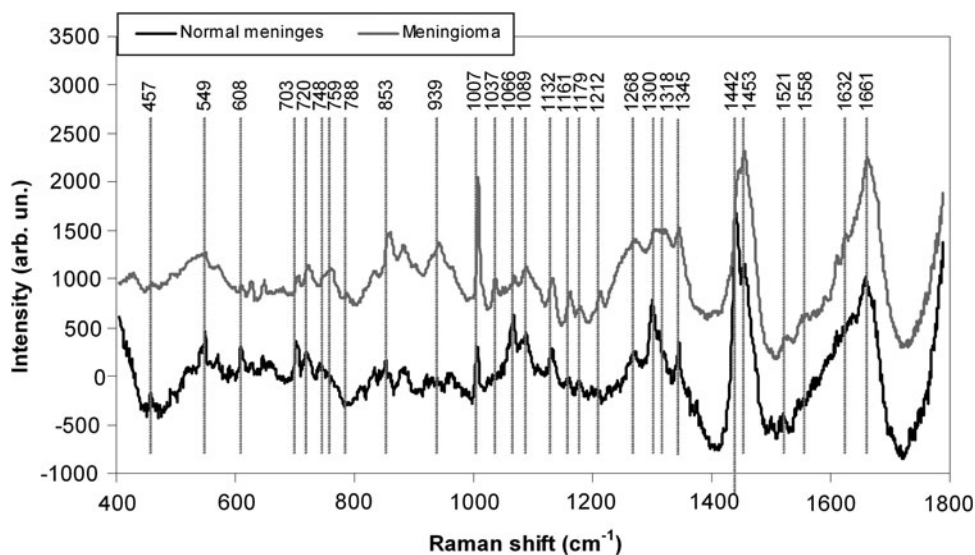
The spectral differences between the different brain tissues provided evidence of biochemical changes associated with the disease, and a possible discrimination of neoplasia from

normal tissues, mainly in bands related to protein, lipids/phospholipids, and cholesterol. These differences were exploited by the discrimination model based on PCA applied to all 172 spectra. It was verified that the first four principal components (PC1 the PC4) carry >95% of all of the spectral variation found in the data. In order to verify which PCs could present the highest discrimination power between groups, they were submitted to ANOVA (5% significance) and the pairs of principal components scores (SCs) with higher statistically significant difference were binary plotted.

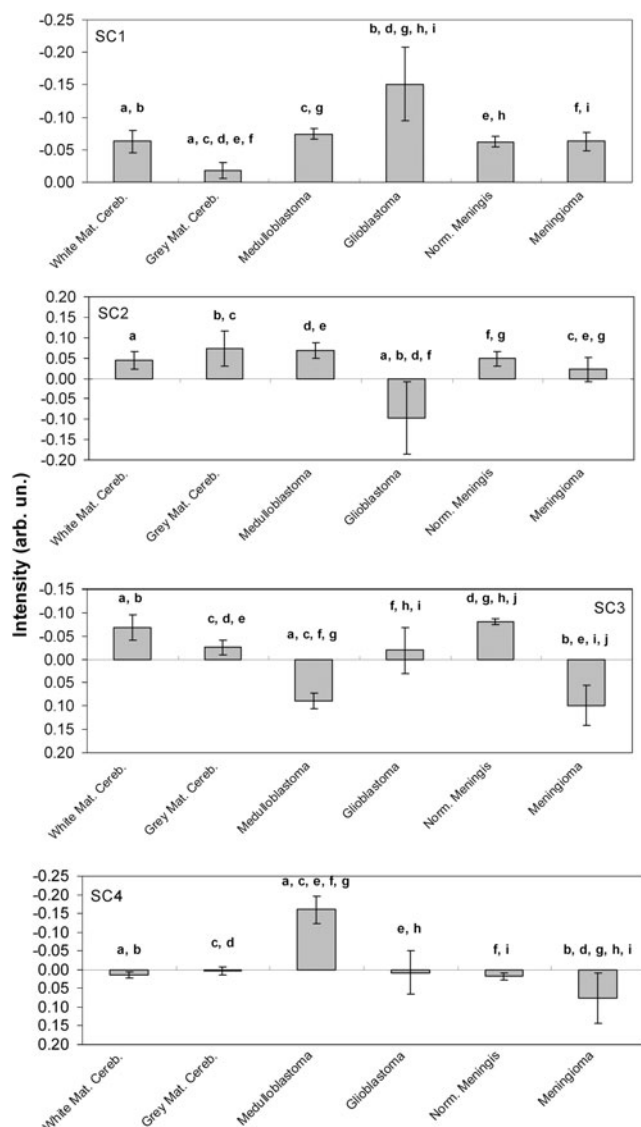
Figure 3 presents the mean intensity and standard deviation of the first four principal components scores (SC1 to SC4) for each tissue type. Statistical analysis indicated that SC1 was effective in discriminating the gray cerebellum and glioblastoma with relation to remnant groups; SC2 was effective in discriminating glioblastoma from other groups except meningioma, meningioma with relation to normal meninges, and medulloblastoma with relation to glioblastoma and meningioma; SC3 was able to better discriminate normal tissues, such as the gray cerebellum and meninges, from tumor tissues, such as the medulloblastoma and meningioma. SC4 was able to discriminate medulloblastoma and meningioma of other groups, including themselves. As SC1 was not able to discriminate meningioma from normal tissue, and SC4 was not able to discriminate glioblastoma from normal tissue, these SCs were not used, and SC2 and SC3 were used.

Figure 4 shows the PCs PC2 and PC3. It was pointed out that PC2 was able to discriminate mainly glioblastoma tumors and other normal tissues; PC2 has spectral characteristics of lipids/phospholipids and cholesterol, which are very intense biochemical components in glioblastoma tumors. It was observed that PC3, which discriminates medulloblastoma and meningioma from normal tissues, has positive peaks related to proteins (meningioma and medulloblastoma are rich in collagen), whereas the negative peaks are related to lipids/phospholipids and, mainly, cholesterol, which are present in these normal tissues (especially the meninges and white cerebellum).

Figure 5 shows the binary plot of the scores SC2 and SC3 for all tissue types and the calculated Euclidean distance for



**FIG. 2.** Mean Raman spectra of normal meninges and meningioma. Spectra were offset for better visualization. Wavelength, 830 nm; laser power, 350 mW; resolution, 2  $\text{cm}^{-1}$ .



**FIG. 3.** Mean intensity and standard deviation of the first four principal components scores (SCs) for each tissue type. Superscript letters in each principal component (PC) indicate groups with statistically significant differences ( $p < 0.05$ ).

group discrimination. Classification showed that, for normal tissues (independently of being cerebellum or meningis), 94 out of 94 spectra presented correct grouping; for medulloblastoma, 17 out of 19 spectra presented correct grouping; for glioblastoma, 16 of 20 spectra presented correct grouping; for meningioma, 35 of 39 spectra presented correct grouping. These results are summarized in Table 2. The Euclidean distance was adequate for the differentiation of the brain tumors from normal tissues. We tested other discriminating functions presented in Matlab's Statistics toolbox: linear, quadratic, and Mahalanobis. Linear and quadratic functions showed similar overall correct classification as did Euclidean, whereas Mahalanobis showed worse results.

The classification results showed high sensitivity and specificity, 97.4% and 100%, respectively, for the diagnosis of brain tumor compared with normal tissue. With relation to tumor medulloblastoma, meningioma, and glioblastoma,

sensitivity varied between 80% and 89.7% and specificity ranging between 97% and 99%.

## Discussion

Brain tissue is constituted mainly of lipids and proteins, and >80% is water.<sup>34</sup> Brain lipids consist mainly of three categories: cholesterol, sphingolipids (sphingomyelin, cerebroside, sulphatides, gangliosides) and glycerophospholipid (phosphatidylcholine, phosphatidylethanolamine, phosphatidylinositol).<sup>35</sup> Raman spectra of normal white and gray cerebellum presented differences between them, demonstrating different biochemical composition. The white part had most of the peaks related to lipids compared with the gray part: peaks assigned to cholesterol, lipids/phospholipids, and proteins, corroborating the recent literature.<sup>29</sup> Raman spectroscopy was able to detect differences in the amounts of these lipids in the white and gray cerebellum.

The distribution of phospholipids in subcellular membranes isolated from human brain depends upon factors such as age, sex, and diet.<sup>36</sup> The concentration of lipids in the white part of the brain in individuals 55 years of age is 64.6% compared with 39.6% of the gray part.<sup>37</sup> The concentration of sphingomyelin in the white part is higher in relation to the gray part (~63.2% and 25.5%, respectively), and the phosphatidylcholine concentration is ~45.2% in the white and 31.4% in the gray part of the brain.<sup>38</sup> The normal brain tissue possesses cholesterol concentrations estimated at 27.5% in the white and 22% in the gray part of the cerebellum.<sup>39</sup>

With respect to the spectral differences of the medulloblastoma compared with the glioblastoma, the latter showed intense peaks across the spectral range related to lipids/phospholipids (881, 1066, 1132, 1300, and 1442  $\text{cm}^{-1}$ ) and particularly cholesterol (549, 703, 881, 962, 1132, and 1442  $\text{cm}^{-1}$ ), whereas medulloblastoma showed higher intensities of the peaks related to protein (1035  $\text{cm}^{-1}$ ) and phospholipids (788  $\text{cm}^{-1}$ ). Biochemical composition of medulloblastoma include cholesterol (22%), lipids (2.2%), and phospholipids (2.4%), phosphatidylcholine (55%) and phosphatidylethanolamine (29%) being the most relevant ones,<sup>39</sup> indicating that Raman bands correlated with known tissue biochemistry. The composition of glioblastoma tissues is mainly cholesterol (23%), phospholipids (2.1%), with phosphatidylcholine (44%), phosphatidylethanolamine (29%), and sphingomyelin (20%) being the most important ones.<sup>39</sup>

Although the most intense protein bands (1318, 1453, and 1661  $\text{cm}^{-1}$ ) overlap with the lipids, it is possible to verify higher amount of proteins in glioblastoma and medulloblastoma tumors by analysis of other important peaks. The peak at 1161  $\text{cm}^{-1}$  (collagen) has higher intensity in these tumors compared with in normal tissue (Fig. 1). The band at 1007  $\text{cm}^{-1}$  (phenylalanine ring) shows an intense peak in the tumors relative to normal tissues. Also, the strong band at the 1440–1460  $\text{cm}^{-1}$  region has the shoulder at 1453  $\text{cm}^{-1}$ , indicating high protein content. These results demonstrated that the spectral differences in the amount of proteins and lipids/phospholipids in tumors and the normal cerebellum are relevant, and that these tissues could be discriminated using Raman technique.

The Raman spectrum of meningioma showed several bands with higher intensity compared with normal meningis, especially the protein peaks (853, 939, 1007, 1032, 1161,

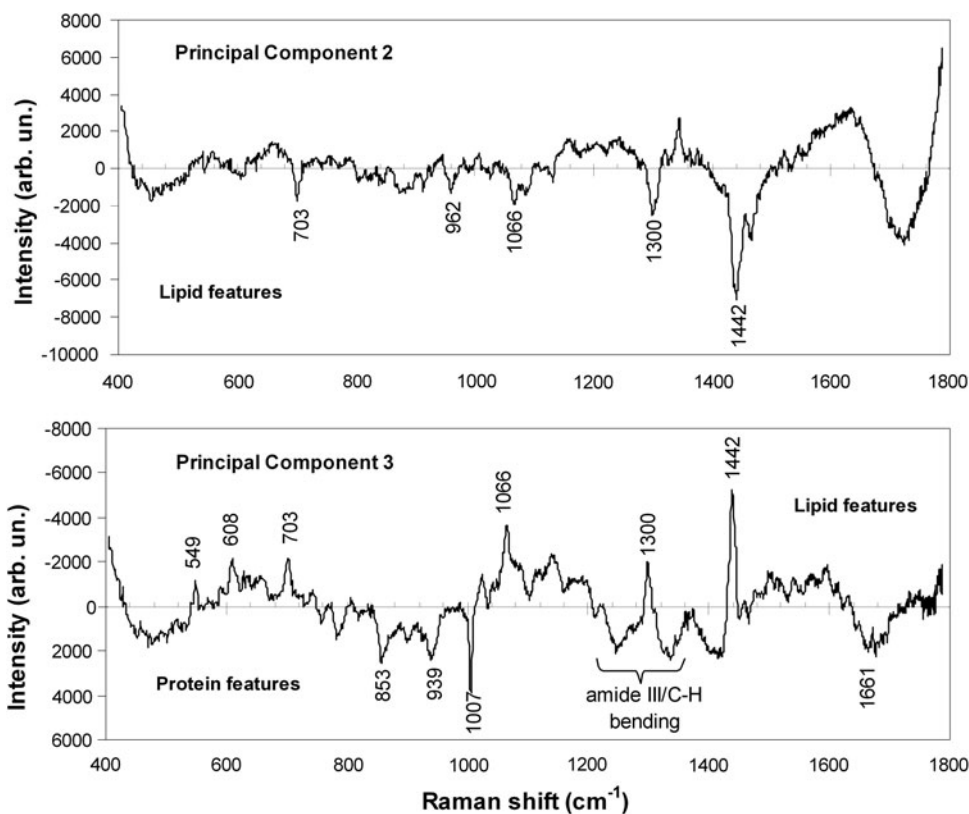


FIG. 4. Principal components spectral vectors PC2 and PC3.

1179, 1268, and 1318  $\text{cm}^{-1}$ ), hemoglobin peak (1212 and 1558  $\text{cm}^{-1}$ ) and lipid/phospholipid peaks (759, 788, and 1268  $\text{cm}^{-1}$ ). The normal meninges showed the most intense bands related to cholesterol and saturated fatty acids (457, 549, 608, 703, 1066, 1300, and 1442  $\text{cm}^{-1}$ ). In meningiomas, bands at 939, 1007, and 1161  $\text{cm}^{-1}$ , indicated the presence of collagen in higher amounts compared with normal meninges. The presence of collagen is consistent with the literature, as meningiomas originate from the meninges, which contain a significant amount of collagen.<sup>13</sup> Collagen (types I, III, and IV) is the most abundant structure in the extracellular matrix of human meninges. In addition to collagen, meningothelial

cells synthesize fibronectin, laminin, and tenascin.<sup>40</sup> Montagnani et al.<sup>41</sup> found that intracranial meninges are rich in collagen type I and IV compared with spinal meninges, which are rich in collagen type III<sup>39</sup>. The expression of different proteins in meningiomas of varying grades was found to be altered, indicating a possible change in their content depending upon tumor grading.<sup>39</sup>

Bands assigned to hemoglobin were observed in all neoplastic tissues. It was found that these hemoglobin peaks (1212, 1226, and 1559  $\text{cm}^{-1}$ ) are more intense in tumors, suggesting greater vascularization, although hemoglobin bands have not been considered relevant for tumor versus

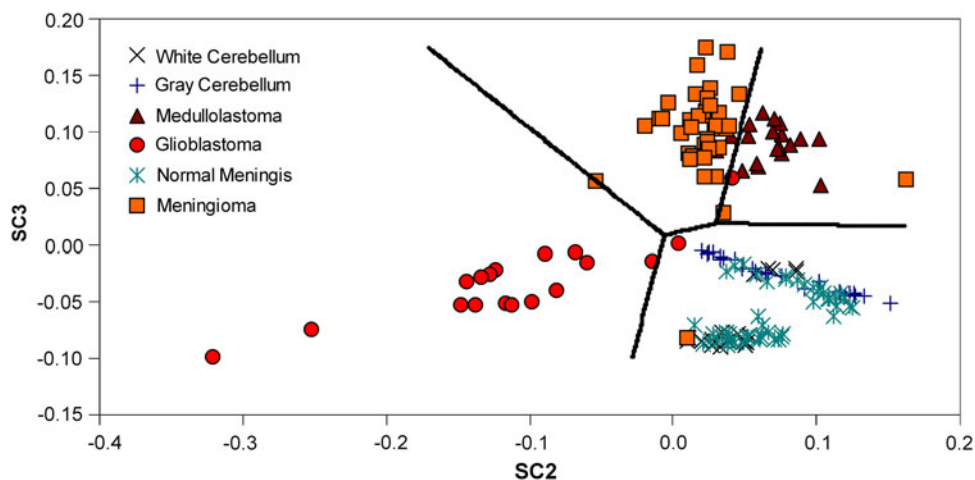


FIG. 5. Plot of the intensities of the principal components scores SC2 and SC3 for the brain tissue groups. The diagnostic line based on the Euclidean distance discriminates the normal brain tissue from glioblastoma, medulloblastoma, and meningioma.

TABLE 2. DISCRIMINATION RESULTS OF THE PRINCIPAL COMPONENT ANALYSIS (PCA)/EUCLIDEAN MODEL APPLIED TO THE RAMAN SPECTRA OF CEREBELLUM AND MENINGES USING PRINCIPAL COMPONENT SCORES SC2 AND SC3

Histopathology	Raman diagnostic based on PCA and Euclidean distance			
	Normal	Medulloblastoma	Glioblastoma	Meningioma
Normal ( $n=94$ )	94	0	0	0
Medulloblastoma ( $n=19$ )	0	17	0	2
Glioblastoma ( $n=20$ )	1	1	16	2
Meningioma ( $n=39$ )	1	2	1	35
Sensibility (%) <sup>a</sup>		89.5	80	89.7
Specificity (%) <sup>a</sup>		98	99	97
Sensibility (%) <sup>b</sup>			97.4	
Specificity (%) <sup>b</sup>			100	
Accuracy (%) <sup>b</sup>			94.2	

<sup>a</sup>Sensitivity and specificity for the diagnosis of each tumor compared with other types of tumor, and normal tissue.

<sup>b</sup>Sensitivity and specificity for the diagnosis of all tumors compared with all normal tissue.

normal classification.<sup>13</sup> The presence of water, with a (weak) band in the region of  $1632\text{ cm}^{-1}$ , may be considered an important feature for brain tissue differentiation. The normal gray cerebellum is  $\sim 82\%$  water and the white is  $\sim 72\%$  water, whereas glioblastoma and medulloblastoma are  $\sim 87\%$  water.<sup>39</sup> Therefore, water could be an important component in the discrimination of tumor tissue from normal tissue. The band at  $1521\text{ cm}^{-1}$  (carotenoids) was found in all normal and tumor samples, being associated with the lipids in brain tissue.<sup>13</sup>

Multivariate techniques such as PCA have been used extensively for identification of spectral differences associated with morphologic changes arising from human diseases, considering that in most cases the changes are subtle and difficult to interpret, and are related to molecular components that are often superimposed. PCA extracts relevant information from the original data, basically the spectral differences between the groups; being able to identify the spectral bands is significant for the diagnosis, as the principal components are related to the biochemical constituents.<sup>8,22,43</sup>

The PCA/Euclidean distance was able to discriminate between the spectra of normal and tumor tissue, despite the small number of samples. The ANOVA applied to the scores of PCs showed that SC2 and SC3 were able to successfully discriminate neoplastic lesions from normal tissues (higher lipid content for glioblastoma, higher protein content for medulloblastoma and meningioma). The false-positive diagnosis presented in this study (2 spectra of medulloblastoma, 4 of glioblastoma, and 4 of meningioma in a total of 172 spectra) were small compared with the correct results, which could be attributed to the sampling method used (random cut) and tissue variability. The diagnosis using the PCA/Euclidean distance applied to Raman spectra showed sensitivity, specificity, and accuracy of 97.4%, 100%, and 94.2%, respectively, considering the normal and all neoplastic tissue groups. Studies with Raman and PCA in other tissues *in vitro* also achieved high sensitivity; for example, the diagnosis of oral carcinoma had 100% sensitivity<sup>40</sup> and discrimination of colon tissue obtained 95% sensitivity.<sup>44</sup>

The gold standard technique used for the differentiation of tumors relative to normal tissue in diagnostic procedures during resection surgery, excisional biopsy followed by histopathologic evaluation, requires time, as seriate samples need to be evaluated in order to evaluate the tumor margins,

which can bring delay and costs associated with the tumor resection surgery procedure. The search for optical techniques in order to obtain spectral information that could be correlated to the histopathology quickly and cost effectively during surgical procedures is challenging. Among these techniques, Raman spectroscopy could assist the identification of tissue composition, correlating the molecular alterations with pathology in different specialties,<sup>7-10</sup> allowing diagnosis *in vivo* in real time.<sup>9</sup> Raman technique may be relevant in determining surgical margins in open skull surgeries, seeing that healthy tissues are not removed in sensitive parts of the human brain, and performing a rapid histopathology after biopsy, reducing the time for diagnosis. A disadvantage is the need for longer exposure time to obtain Raman images of larger areas.

The results obtained in this study showed that Raman spectroscopy can identify changes in the concentration of biochemicals presented in neoplastic and normal tissues and, associated with a discriminant analysis technique such as PCA/Euclidean distance, can become a powerful and reliable tool for a biochemical diagnosis of brain lesions.

## Conclusions

This study showed that Raman spectroscopy is an effective technique for detecting biochemical changes in glioblastoma, medulloblastoma and meningioma brain tumors, and comparing them with normal brain tissues from the cerebellum and meninges, indicating different concentrations of lipids/phospholipids, cholesterol, proteins, and hemoglobin in neoplastic tissues of the cerebellum and meninges. The diagnosis using PCA/Euclidean distance, using the spectral differences contained in the principal component scores SC2 and SC3, showed a sensitivity and specificity of 97.4% and 100%, respectively, for discriminating tumors from normal tissues.

## Acknowledgment

Dr. thanks FAPESP (São Paulo Research Foundation) for partial financial support (Proc. no. 2009/01788-5).

## Author Disclosure Statement

No competing financial interests exist.

## References

1. Instituto Nacional de Câncer José Alencar Gomes da Silva - INCA (2011). Estimate/2012 - Cancer Incidence in Brazil. Available at: <http://www.inca.gov.br/estimativa/2012/estimativa20122111.pdf> Accessed May 30, 2012.
2. Stone, N., Crow, P., Hart, P.M.C., and Ritchie, A.W. (2007). The use of Raman spectroscopy to provide an estimation of the gross biochemistry associated with urological pathologies. *Anal. Bioanal. Chem.* 387, 1657–1688.
3. Vargis, E., Jasen, A.M., Tang, Y.W., and Khabele, D. (2012). Near-infrared Raman microspectroscopy detects high-risk human papillomaviruses. *Transl. Oncol.* 5, 172–179.
4. Huang, Z., Teh, S.K., Zheng, W., Lin, K., Ho, K.Y., The, M., and Yeoh, K.G. (2010). In vivo detection of epithelial neoplasia in the stomach using image-guided Raman endoscopy. *Biosens. Bioelectron.* 269, 383–3895.
5. Jansen, M.A., Keller, D.M., Vargis, E., Granja, N.M., Wilson, R.H., Mycek, M.A., and Kelley, M.C. (2011). Development of a spatially offset Raman spectroscopy probe for breast tumor surgical margin evaluation. *J. Biomed. Opt.* 16, 077006.
6. Kanter, E.M., Majumder, S., Vargis, E., Robichaux, V.A., Kanter, G.J., Shappell, H., Jones, H.W., and Mahadevan, J.A. (2009). Multiclass discrimination of cervical precancers using Raman spectroscopy. *J. Raman. Spectrosc.* 40, 205–211.
7. Haka, A.S., Nazemi, J., Volynskaya, Z., Gardecki, J.A., Shenk, R., Wang, N., Dasari, R.R., Fitzmaurice, M., and Feld, M.S. (2009). Diagnosing breast cancer using Raman spectroscopy: prospective analysis. *J. Biomed. Opt.* 14, 054023.
8. Silveira, L., Silveira, F.L., Bodanese, B., Zângaro, R.A., and Pacheco, M.T.T. (2012). Discriminating model for diagnosis of basal cell carcinoma and melanoma in vitro based on the Raman spectra of selected biochemicals. *J. Biomed. Opt.* 17, 077003.
9. Halon, E.B., Manoharan, R., Koo, T.H., Shafer, K.E., Motz, J.T., Fitzmaurice, M., Kramer, J.R., Itzkan, I., Dasari, R.R., and Feld, M.S. (2000). Prospects for in vivo Raman spectroscopy. *Phys. Med. Biol.* 45, R1–R59.
10. Stone, N., Kendall, C., Smith, J., Crow, P., and Barr, H. (2004). Raman spectroscopy for identification of epithelial cancers. *Faraday Discuss.* 126, 141–157.
11. Beljebbar, A., Dukic, S., Amharref, N., and Manfait, M. (2010). Ex vivo and in vivo diagnosis of C6 glioblastoma development by Raman spectroscopy coupled to a microprobe. *Anal. Bioanal. Chem.* 398, 477–487.
12. Koljenović, S., Smith, L.P., Bakker, S.T.C., Kros, J.M., Berge, H.J., and Puppels, G.J. (2002). Discriminating vital tumor from necrotic tissue in human glioblastoma tissue samples by Raman spectroscopy. *Lab. Invest.* 82, 1265–1267.
13. Krafft, C., Sobottka, S.B., Schackert, G., and Salzer, R. (2005). Near infrared Raman spectroscopic mapping of native brain tissue and intracranial tumors. *Analyst* 130, 1070–1077.
14. Kirsch, M., Schackert, G., Salzer, R., and Krafft, C. (2010). Raman spectroscopic imaging for in vivo detection of cerebral brain metastases. *Anal. Bioanal. Chem.* 398, 1707–1713.
15. Beleites, C., Geiger, K., Kirsch, M., Sobottka, S.B., Schackert, G., and Salzer, R. (2011). Raman spectroscopic grading of astrocytoma tissues: using soft reference information. *Anal. Bioanal. Chem.* 400, 2801–2816.
16. Krafft, C., Belay, B., Bergner, N., Romeike, B.F., Reichart, R., Kalff, R., and Popp, J. (2012). Advances in optical biopsy – correlation of malignancy and cell density of primary brain tumors using Raman microspectroscopic imaging. *Analyst* 137, 5533–5537.
17. Leslie, D.G., Kast, R.E., Poulik, J.M., Rabah, R., Sood, S., Auner, G.W., and Klein, M.D. (2012). Identification of pediatric brain neoplasms using Raman spectroscopy. *Pediatr. Neurosurg.* 48, 109–117.
18. Zhou, Y., Liu, C.H., Sun, Y., Pu, Y., Boydston-White, S., Liu, Y., and Alfano, R.R. (2012). Human brain cancer studied by resonance Raman spectroscopy. *J. Biomed. Opt.* 17, 116021.
19. Dunteman, G.H. (1989). Principal components analysis. Newbury Park: Sage Publications.
20. Maheedhar, K., Pujary, P., Krishna, C.M., and Pujary, K. (2011). Raman spectroscopic methods classification of normal and malignant hypopharyngeal tissues: An exploratory study. *Patholog. Res. Int.* 2011, 632493.
21. Harris, A.T., Garg, M., Yang, X.B., Fisher, S.E., Kirkham, J., Smith, D.A., Hirsch, D.P.M., and High, A.S. (2009). Raman spectroscopy and advance mathematical modeling in the discrimination of human thyroid cell lines. *Head Neck Oncol.* 1, 1–6.
22. Bodanese, B., Silveira, F.L., Zângaro, R.A., Pacheco, M.T., Pasqualucci, C.A., and Silveira, L. (2012). Discrimination of basal cell carcinoma and melanoma from normal skin biopsies in vitro through Raman spectroscopy and principal component analysis. *Photomed. Laser Surg.* 30, 381–387.
23. Teh, S.K., Zheng, W., Ho, K.Y., Teh, M., Yeoh, K.G., and Huang, Z. (2010). Near-infrared Raman spectroscopy for early diagnosis and typing of adenocarcinoma in the stomach. *Br. J. Surg.* 97, 550–557.
24. Nogueira, G.V., Silveira, L., Martin, A.A., Zângaro, R.A., Pacheco, M.T., Chavantes, M.C., and Pasqualucci, C.A. (2005). Raman spectroscopy study of atherosclerosis in human carotid artery. *J. Biomed. Opt.* 10, 031117.
25. Louis, D.N., Ohgaki, H., Wiestler, O.D., Cavenee, W.K., Burger, P.C., Jouvet, A., Scheithauer, B.W., and Kleihues, P. (2007). WHO classification of tumors of the central nervous system. *Acta Neuropathol.* 114, 97–109.
26. McCreery, R.L. (2000). Raman spectroscopy for chemical analysis. Danvers: Wiley Interscience.
27. Black, P.E. (2004). Euclidean distance. U.S. National Institute of Standards and Technology. Available at: <http://www.nist.gov/dads/HTML/euclidndstnc.html> Accessed October 29, 2012.
28. Krafft, C., Neudert, L., Simat, T., and Salzer, R. (2005). Near infrared Raman spectra of human brain lipids. *Spectrochim. Acta A: Mol. Biomol. Spectrosc.* 61, 1529–1535.
29. Dreissig, I., Machill, S., Salzer, R., and Krafft, C. (2009). Quantification of brain lipids by FTIR spectroscopy and partial least squares regression. *Spectrochim. Acta A: Mol. Biomol. Spectrosc.* 71, 2069–2075.
30. Köhler, M., Machill, S., Salzer, R., and Krafft, C. (2009). Characterization of lipid extracts from brain tissue and tumors using Raman spectroscopy and mass spectrometry. *Anal. Bioanal. Chem.* 393, 1513–1520.
31. Meyer, T., Bergner, N., Bielecki, C., Krafft, C., Akimov, D., Romeike, B.F.M., Reichart, R., Kalff, R., Dietzek, B., and Popp, J. (2011). Nonlinear microscopy, infrared, and Raman microspectroscopy for brain tumor analysis. *J. Biomed. Opt.* 16, 021113.
32. Schrader, B. (1989). Raman/infrared atlas of organic compounds. New York: VCH.
33. Movasaghi, Z., Rehman, S., and Rehman, I.U. (2007). Raman spectroscopy of biological tissues. *Appl. Spectrosc. Rev.* 42, 493–541.
34. Suzuki, K. (1981). Chemistry and metabolism of brain lipids, in: *Basic Neurochemistry*, 3rd ed. G.J. Siegel, R.W. Albers, B.W.

- Agranoff, and R. Katzman (eds.). Boston: Little, Brown and Company, pp. 355–370.
35. Quarles, R., Macklin, W., and Morell, P. (2005). Myelin formation, structure and biochemistry, in: *Basic Neurochemistry: Molecular, Cellular and Medical Aspects*. R.W. Albers (ed.). Burlington: Elsevier, pp. 51–72.
  36. Sun, G.Y. (1973). Phospholipids and acyl groups in subcellular fractions from human cerebral cortex. *J. Lipid Res.* 14, 656–663.
  37. Brien, J.S., and Sampson, E.L. (1965). Lipid composition of the normal human brain: gray matter, white matter, and myelin. *J. Lipid Res.* 6, 537–544.
  38. Brien, J.S., and Sampson, E.L. (1965). Fatty acid and fatty aldehyde composition of the major brain lipids in normal human gray matter, white matter, and myelin. *J. Lipid Res.* 6, 545–551.
  39. Yates, A.J., Thompson, D.K., Boesel, C.P., Albrightson, C., and Hart, R.W. (1979). Lipid composition of human neural tumors. *J. Lipid Res.* 20, 428–436.
  40. Lopes, M.B.S. (2009). Meninges embryology, in: *Meningiomas: Diagnosis, Treatment and Outcome*. J.H. Lee (ed.). London: Springer, pp. 25–30.
  41. Montagnani, S., Castaldo, S., Meglio, F.D., Sciorio, S., and Lanza, G.G. (2000). Extra cellular matrix features in human meninges. *Ital. J. Anat. Embryol.* 105, 167–177.
  42. Okamoto, H., Li, J., Vortmeyer, A.O., Jaffe, H., Lee, Y.S., Gläsker, S., Sohn, T.S., Zeng, W., Ikejiri, B., Proescholdt, M.A., Mayer, C., Weil, R.J., Oldfield, E.H., and Zhuang, Z. (2006). Comparative proteomic profiles of meningioma subtypes. *Cancer Res.* 66, 10,199–10,204.
  43. Silveira, L., Oliveira, A.P., Bitar, R.A., Zângaro, R.A., and Martin, A.A. (2006). Near-infrared Raman spectroscopy for oral carcinoma diagnosis. *Photomed. Laser Surg.* 24, 348–353.
  44. Chowdary, M.V., Kumar, K.K., Thakur, K., Anand, A., Kurien, J., Krishna, C.M., and Mathew, S. (2007) Discrimination of normal and malignant mucosal tissues of the colon by Raman spectroscopy. *Photomed. Laser Surg.* 25, 269–274.

Address correspondence to:

Landulfo Silveria, Jr.  
Biomedical Engineering Institute  
Universidade Camilo Castelo Branco  
São José dos Campos, SP  
Brazil

E-mail: landulfo.silveira@gmail.com